JOURNAL OF COMPUTATIONAL PHYSICS 63, 398–415 (1986)

SIMM1: A Linearized Particle Code

GLENN JOYCE AND MARTIN LAMPE

Plasma Theory Branch, Plasma Physics Division, Naval Research Laboratory, Washington, D.C. 20375

Received September 26, 1984; revised June 12, 1985

SIMM1 is a linearized particle simulation code used to study the resistive hose instability of a self-pinched relativistic electron beam propagating in resistive plasma. The code treats the zero-order axisymmetric beam dynamics as a group of macroparticle rings. The particle dynamics associated with the hose perturbations is represented by linearized displacements of these rings from the beam axis and by bunching of the charge density around the ring. The linearization procedure presents difficulties which must be dealt with to determine the long-time behavior of the system. The axisymmetric motion of the rings occurs under the influence of an anharmonic central potential which leads to secular behavior of the orbit perturbations. We have developed a method of coarse graining to deal with the problem of secularities.
© 1986 Academic Press, Inc.

I. INTRODUCTION

Self-pinched relativistic electron beams propagating in resistive plasma are subject to the resistive hose instability, essentially a growing snakelike oscillation which is often observed to destroy the integrity of the beam [1]. For this instability, the linear regime (small instability amplitude) is of particular interest, because the mode grows convectively backward in the beam, and therefore it is possible within the linear regime for the instability amplitude at any given location in the beam to reach a maximum level and then decay.

A variety of analytic techniques have been used to study the linearized hose instability [2–7], but these approaches have not been able to treat an essential feature of the problem, namely that self-pinched beams generally are not in time-independent equilibrium. The very front of the beam head is always unpinched and therefore continuously erodes away; also the beam radius increases steadily due to scattering off gas molecules, and the particle energy decreases and spreads due to various loss mechanisms. Even the radial profile of the beam density may change with time and from place to place in the beam.

Two approximate numerical models have also been developed previously to simulate the space–time evolution of the linearized resistive hose instability [8, 7]. In these treatments, the actual particle dynamics is replaced by simplified macroscopic models, which are carefully chosen to preserve a key feature of the dynamics, the spread in betatron oscillation frequency among the electrons follow-

0021-9991/86 $3.00
Copyright © 1986 by Academic Press, Inc.
All rights of reproduction in any form reserved.

ing various oscillation orbits in the pinched beam. [If this feature were absent from the model, the hose instability would erroneously become absolute rather than convective [4]]. The macroscopic models are capable of treating time-dependent equilibria, but they are limited to cases where the equilibrium beam density profile $n_b(r, z, t)$ has the self-similar form $n_b[r/a(z, t)]$, and furthermore the accuracy of the models has been demonstrated only for cases where this profile has the Bennett form, $n_b = n_{b0}[1 + r^2/a^2(z, t)]^{-2}$. However, the actual radial density profile of a self-pinched beam may be hollow, or may have wings of significant amplitude at large radius, or may (on the other hand) be cut-off sharply at some radius, or may vary greatly in shape from place to place in the beam. These types of details of the equilibrium, which cannot be represented in any of the existing models, can strongly affect the growth of the hose mode.

The technique generally used to study instabilities in temporally and spatially varying situations is particle simulation, but in practice a standard unlinearized simulation using any reasonable number of simulation particles (e.g., 10^6 or even more) might have a noise level large enough to mask or misrepresent the instability in the linear regime. To overcome these problems and to provide a very general treatment of the resistive hose, we have developed a *linearized* particle simulation code, which successfully determines both growth rates and saturation amplitudes during the small-amplitude stage of the instability [9]. The techniques used, which build upon the earlier work of Friedman, Denavit, and Sudan [10] may also be applicable to other instabilities which grow out of complicated or time-varying equilibria. Chambers, Masamitsu, and Lee have also developed a linearized particle simulation code to treat hose instability [11]. Their work is similar to ours in some ways and differs in other ways, e.g., they do not use the "coarse-graining " technique described in this paper.

The code, SIMM1, treats the zero-order axisymmetric beam dynamics ($m = 0$, where the azimuthal dependence is Fourier analyzed into $e^{im\theta}$ dependence) as a group of axisymmetric macroparticle rings. This portion of the code is named SIMMO and has been discussed in a previous publication [12]. The $m = 1$ particle dynamics associated with the hose perturbations is represented by linearized displacements of these rings from the beam axis and by $m = 1$ bunching of the charge density around the ring.

A large number of these rings are followed in time as they interact with each other and with the background gas. The beam is assumed to be highly relativistic so that quantities of the order of $\gamma^{-2} \equiv 1 - v^2/c^2$ are neglected. The paraxial approximation is also made, i.e., the axial velocities of the particles are taken to be c, and the perpendicular velocities are assumed to be small. The dynamics of the particles' motions are determined from solutions of Maxwell's equations. A simplified form of Maxwell's equations is appropriate to highly relativistic, paraxial beams[13]. The equations are presented in Appendix A. The beam travels through a gas which is assumed to be highly collisional and so dense that its mass motions can be neglected on the beam time scale. The beam partially ionizes the gas which, in turn, provides charge neutralization and allows the beam to self-pinch in its own

magnetic field. The gas is modeled as a stationary conducting medium with a local scalar conductivity which is determined by the process of beam-impact ionization, avalanche ionization (when there are large beam-generated electric fields), and recombination. Conductivity physics can be modeled at various levels of sophistication. The model used in SIMM1 is discussed in Appendix A. The code, then, consists of axisymmetric dynamics, linearized $m = 1$ dynamics, electromagnetic field generation, and interactions with the background gas.

The linearization procedure presents difficulties which must be dealt with to determine the long-time behavior of the system. The zero-order axisymmetric motion of the rings occurs under the influence of an anharmonic central potential, so the period of their motion depends on the oscillation amplitude. Within a linearized model, this effect leads to secular behavior of the $m = 1$ perturbations to the orbits. With a large enough number of particles, the individual orbit secularities would average out to yield nonsecular macroscopic quantities, but to run a practical simulation some method of suppressing the long-time orbit secularities must be employed. We have developed a method of coarse graining to deal with this problem.

We will discuss the linearization process in Section II; the problem of secular behavior and its resolution by coarse graining in Section III. Details are given in Appendices A and B.

II. Code Structure

SIMM1 is greatly simplified by our approximation that all particles have axial velocity c, so that no particle overtaking is permitted along the beam axis. As a result, we can consider the beam to be made up of a series of slices of particles stacked along the beam axis from its head to its tail. The simulation can be thought of as a number of two-dimensional (r, θ) simulations, with information carried along the axis by the fields and conductivity.

We use as our independent variables r, θ, $\zeta \equiv ct - z$, and z where t is the time and ct is the position of the beam head in space. The coordinate ζ is a measure of the distance along the axis from the beam head. In this set of coordinates, z acts as a time-like variable with regard to beam dynamics, while ζ is a constant of the motion for any particle.

A. *Particle Dynamics*

The beam particle dynamics is represented in terms of the motion of particle rings under the $m = 0$ and $m = 1$ forces. Each ring represents the set of all particles with the same initial value of r, ζ, radial velocity, and angular momentum. It is obvious that under the influence of an axisymmetric force the $m = 0$ motion of this set of particles is such that it remains a ring, with radius increasing or decreasing in time. To calculate the $m = 0$ dynamics of the ring, it is thus sufficient to follow the dynamics of any one particle on the ring. It is more convenient to do this in Cartesian coordinates in the $r - \theta$ plane; our method is described elsewhere [12].

To first order in treating the $m = 1$ perturbations, each particle can be assigned a small time-dependent displacement from its equilibrium orbit in the $r - \theta$ plane. Friedman *et al.* [10] have shown that to first order the set of particles forming any given ring still lie on a circular ring, but that the center of the ring is displaced from the origin by a small vector quantity, and that in addition the charge density around the ring is no longer uniform, but rather is (slightly) bunched as $e^{i(\theta - \theta_0)}$. The linearized $m = 1$ dynamics of all particles in the ring is thus characterized by four time-dependent quantities: the two components of the displacement of the ring center, the bunching axis θ_0, and the amplitude of the bunching. These four quantities can be represented in various ways; the following scheme is one way of doing this and of tying the dynamics of the whole ring to that of one reference particle on it.

Figure 1 shows the equilibrium and perturbed positions of some ring. R and P are two particles on the perturbed ring, and R' and P' are the perturbed positions of these particles. We represent the line segment $\overline{RR'} = \mathrm{Re}\,(\varepsilon(R))$. The quantity $\varepsilon(R)$ is the perturbation of the ring at the point R. In the same manner the line segment $\overline{PP'} = (\varepsilon(P))$. Note that the arc $\overline{RP}$ may not be the same length as the arc $\overline{R'P'}$, since the ring of charge is bunched as well as displaced.

It can be shown Friedman *et al.* [10] that if we choose the relationship between $\varepsilon(R)$ and $\varepsilon(P)$ to be given by

$$\varepsilon_r(P) = \varepsilon_r(R)e^{i\phi}$$

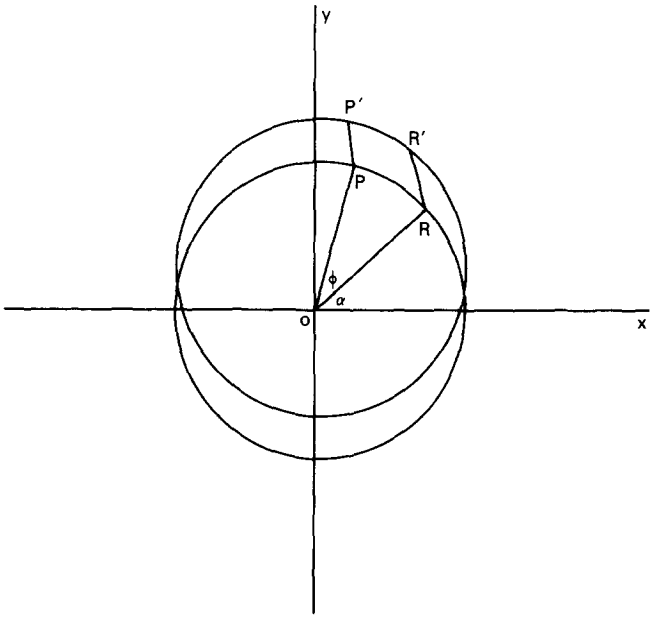

FIG. 1. Schematic of an axisymmetric and a perturbed electron ring. The reference points R and P on the unperturbed ring map into the points R' and P' on the perturbed ring.

and

$$\varepsilon_\theta(P) = \varepsilon_\theta(R)e^{i\phi},$$

where ϕ is the azimuthal separation of P and R, the motions of the perturbations are consistent with the dynamics of the $m = 1$ fields and that we only need to follow the dynamics of the perturbation at a single reference point R. The two *complex* quantities ε_r and ε_θ thus contain all the information about the bunching and displacement of the ring.

Although we have chosen a complex representation of the perturbations, physical quantities must be real. If we let

$$\boldsymbol{\varepsilon} = \boldsymbol{\varepsilon}^r + i\boldsymbol{\varepsilon}^i,$$

we can write

$$\begin{aligned}\overline{PP'} &= \mathrm{Re}\,(\boldsymbol{\varepsilon}(R)e^{i\phi}) \\ &= (\varepsilon_r^r \cos\phi - \varepsilon_r^i \sin\phi, \varepsilon_\theta^r \cos\phi - \varepsilon_\theta^i \sin\phi).\end{aligned}$$

We choose to identify $\varepsilon_r^{\mathrm{I}} = \varepsilon_r^r(R)$, $\varepsilon_r^{\mathrm{II}} = -\varepsilon_r^i(R)$, $\varepsilon_\theta^{\mathrm{I}} = \varepsilon_\theta^r(R)$, and $\varepsilon_\theta^{\mathrm{II}} = -\varepsilon_\theta^i(R)$. Thus

$$\overline{PP'} = (\varepsilon_r^{\mathrm{I}} \cos\phi + \varepsilon_r^{\mathrm{II}} \sin\phi, \varepsilon_\theta^{\mathrm{I}} \cos\phi + \varepsilon_\theta^{\mathrm{II}} \sin\phi).$$

The particle dynamics are computed in Cartesian coordinates. In that coordinate system, we need to follow the four quantities $\varepsilon_x^{\mathrm{I}}$, $\varepsilon_y^{\mathrm{I}}$, $\varepsilon_x^{\mathrm{II}}$, $\varepsilon_y^{\mathrm{II}}$, defined by

$$\begin{aligned}\varepsilon_r^{\mathrm{I,II}} &= \varepsilon_x^{\mathrm{I,II}} \cos\alpha + \varepsilon_y^{\mathrm{I,II}} \sin\alpha, \\ \varepsilon_\theta^{\mathrm{I,II}} &= -\varepsilon_x^{\mathrm{I,II}} \sin\alpha + \varepsilon_y^{\mathrm{I,II}} \sin\alpha,\end{aligned}$$

where α is the azimuthal coordinate of the reference particle R.

We use an approximation to Maxwell's equations that was first derived by Lee [13] and is reasonable for an ultrarelativistic beam in a collisional gas. These equations are given in Appendix A along with a simplified conductivity equation which models direct ionization, avalanche ionization and recombination of the background gas.

We consider only beam perturbations linearly polarized along the y axis. For this case the linearized current density and conductivity are

$$J_{bz} = J_{bz}^0 + J_{bz}^1 \sin\theta,$$

and

$$\sigma = \sigma^0 + \sigma^1 \sin\theta.$$

The only nonzero electric and magnetic fields are

$$B_\theta = B_\theta^0 + B_\theta^1 \sin\theta,$$
$$B_r = B_r^1 \cos\theta,$$
$$E_z = E_z^0 + E_z^1 \sin\theta,$$
$$E_r = E_r^0 + E_r^1 \sin\theta,$$
$$E_\theta = E_0^1 \cos\theta.$$

We use the notation introduced for the ε's to write

$$J_{bz} = J_{bz}^0 + J_{bz}^{II} \sin\theta,$$
$$\sigma = \sigma^0 + \sigma^{II} \sin\theta,$$
$$B_\theta = B_\theta^0 + B_\theta^{II} \sin\theta,$$
$$B_r = B_r^I \cos\theta,$$
$$E_z = E_z^0 + E_z^{II} \sin\theta$$
$$E_r = E_r^0 + E_r^{II} \sin\theta,$$
$$E_\theta = E_\theta^I \cos\theta.$$

The equations of motion of the perturbations are then

$$\begin{aligned}
\frac{m_0c^2}{q}\frac{d}{dz}(\gamma\dot{\varepsilon}_x^I) &= E_r^{II}\sin\alpha\cos\alpha - E_\theta^I\cos\alpha\sin\alpha \\
&\quad - cB_r^I\sin\alpha\cos\alpha - cB_\theta^{II}\cos\alpha\sin\alpha \\
&\quad + (\varepsilon_x^I\cos^2\alpha + \varepsilon_y^I\cos\alpha\sin\alpha)\left(\frac{\partial E_r^0}{\partial r} - c\frac{\partial B_\theta^0}{\partial r}\right) \\
&\quad + (\varepsilon_x^I\sin^2\alpha - \varepsilon_y^I\cos\alpha\sin\alpha)\,(E_r^0/r - cB_\theta^0/r), \\
\frac{m_0c^2}{q}\frac{d}{dz}(\gamma\dot{\varepsilon}_x^{II}) &= E_r^{II}\cos^2\alpha + E_\theta^I\sin^2\alpha \\
&\quad + cB_r^I\sin^2\alpha - cB_\theta^{II}\cos^2\alpha \\
&\quad + (\varepsilon_x^{II}\cos^2\alpha + \varepsilon_y^{II}\cos\alpha\sin\alpha)\left(\frac{\partial E_r^0}{\partial r} - \frac{\partial B_\theta^0}{\partial r}\right) \\
&\quad + (\varepsilon_x^{II}\sin^2\alpha - \varepsilon_y^{II}\cos\alpha\sin\alpha)\,(E_r^0/r - cB_\theta^0/r), \\
\frac{m_0c^2}{q}\frac{d}{dz}(\gamma\dot{\varepsilon}_y^I) &= E_r^{II}\sin^2\alpha + E_0^I\cos^2\alpha \\
&\quad + cB_r^I\cos^2\alpha - cB_\theta^{II}\sin^2\alpha \\
&\quad + (\varepsilon_x^I\sin\alpha\cos\alpha + \varepsilon_y^I\sin^2\alpha)\left(\frac{\partial E_r^0}{\partial r} - c\frac{\partial B_\theta^0}{\partial r}\right) \\
&\quad + (\varepsilon_y^I\cos^2\alpha - \varepsilon_y^I\cos\alpha\sin\alpha)\,(E_r^0/r - cB_\theta^0/r),
\end{aligned}$$

and

$$\frac{m_0 c^2}{q}\frac{d}{dz}(\gamma\dot{\varepsilon}_y^{II}) = E_r^{II}\cos\alpha\sin\alpha - E_\theta^{I}\cos\alpha\sin\alpha$$
$$- cB_r^{I}\sin\alpha\cos\alpha - cB_\theta^{II}\cos\alpha\sin\alpha$$
$$+ (\varepsilon_x^{II}\sin\alpha\cos\alpha + \varepsilon_y^{II}\sin^2\alpha)\left(\frac{\partial E_r^0}{\partial r} - c\frac{\partial B_\theta^0}{\partial r}\right)$$
$$+ (\varepsilon_y^{II}\cos^2\alpha - \varepsilon_x^{II}\cos\alpha\sin\alpha)(E_r^0/r - cB_\theta^0/r)$$

where $\dot{\varepsilon} \equiv d\varepsilon/dz$.

These four complicated equations form the basis of the perturbation dynamics. Although the total beam perturbation is along the y axis, the motion of any single ring is such that its center can lie at any point off the axis. Only in adding all the ring positions together do we get the effects of the simplified perturbation. Otherwise stated, a single ring has angular momentum, so its motion does not in general have the same symmetry as the driving fields; however (it is tacitly assumed) the distribution over angular momentum is even, which restores the symmetry of the beam as a whole.

B. *Current Density*

In the paraxial approximation, the beam current density component J_z along the axis is proportional to the charge density and the components of **J** perpendicular to the axis are neglected. The charge density for a beam made up of point particles formed into rings can be written as

$$J_z(r,\theta) = \sum_k \frac{q_k c}{2\pi}\int_0^{2\pi}\frac{1}{r_k(\phi)}\delta(r - r_k(\phi))\,\delta(\theta - \theta_k(\phi))\,d\phi,$$

where the sum is over the rings and the angle ϕ is the azimuthal angle of Fig. 1. The $r_k(\phi)$ represents the displacement of the ring from the axis and $\theta_k(\phi)$ represents charge bunching.

For a system of finite sized particles, the δ-function $\delta(r - r_k(\phi))$ is replaced by a particle shape function $S_r(r - r_k(\phi))$. Within the framework of the linearization procedure, we can write

$$r_k(\phi) = r_k^0 + \varepsilon_{rk}e^{i\phi},$$
$$\theta_k(\phi) = \theta_k + \varepsilon_{\theta k}e^{i\phi}/r_k^0,$$
$$S_r(r - r_k(\phi)) = S_r(r - r_k^0) - \varepsilon_{rk}e^{i\phi}\frac{\partial S_r}{\partial r_k^0}(r - r_k^0),$$
$$\delta(\theta - \theta_k(\phi)) = \delta(\theta - \theta_k^0) - \varepsilon_{\theta k}e^{i\phi}/r_k^0\delta'(\theta - \theta_k^0).$$

The zeroth- and first-order current densities can be written

$$J_z^0(r) = \sum_k \frac{q_k c}{2\pi r} S_r(r - r_k^0),$$

$$J_z^1 e^{i\theta} = -\sum_k \frac{q_k c}{2\pi r} S_r(r - r_k^0) \frac{\varepsilon_{\theta k}}{r_k^0} ie^{i(\theta - \alpha_k)} - \sum_k \frac{q_k c}{2\pi r} \frac{\partial S_r}{\partial r_k^0} (r - r_k^0)\, \varepsilon_{rk} e^{i(\theta - \alpha_k)}.$$

Finally, we can write the current density as a real function consistent with beam displacements in the y direction as

$$\begin{aligned} J_z = &-\sum_k \frac{q_k c}{2\pi r} S_r(r - r_k^0) \frac{1}{r_k^0} [-(-\varepsilon_{xk}^{\mathrm{I}} \sin \alpha_k + \varepsilon_{yk}^{\mathrm{I}} \cos \alpha_k) \cos \alpha_k \\ &+ (-\varepsilon_{xk}^{\mathrm{II}} \sin \alpha_k + \varepsilon_{yk}^{\mathrm{II}} \cos \alpha_k) \sin \alpha_k] \\ &+ \sum_k \frac{q_k c}{2\pi r} \frac{\partial S_r}{\partial r_k^0} [(\varepsilon_{xk}^{\mathrm{I}} \cos \alpha_k + \varepsilon_{yk}^{\mathrm{I}} \sin \alpha_k) \sin \alpha_k \\ &+ (\varepsilon_{xk}^{\mathrm{II}} \cos \alpha_k + \varepsilon_{yk}^{\mathrm{II}} \sin \alpha_k) \cos \alpha_k]. \end{aligned}$$

Since the perturbation current density contains derivatives of the particle shape, a shape function with continuous derivatives is necessary. We have chosen a quadratic particle interpolation scheme as suggested by Friedman *et al.* [10].

III. Coarse Graining

Although formally we have derived a set of equations to describe the motions of the perturbation quantities, the nature of the beam particle motion results in the breakdown of the linearization procedure under some circumstances. The perturbation of each *individual* particle ring grows without bound even in the absence of $m = 1$ forces. To visualize this behavior, we consider the simpler problem of motion of particles in a *fixed* axisymmetric potential. (Since information only propagates backwards in a beam moving at $v_z = c$, this is equivalent to the problem of the motion of the first perturbed slice of the beam, which is subject to axisymmetric fields determined by the previous unperturbed beam slices.)

The motion of a beam particle in the plane perpendicular to the beam axis, subject to an anharmonic potential well, is quite complicated. In general, the particle will trace out an unclosed rosette orbit. The essential feature, however, is that the radial oscillation period and the azimuthal drift rate depend on the particle's angular momentum and the amplitude of the orbit. Because of this dependence, two particles whose amplitudes are infinitely infinitesimally different will separate in

time until their separation becomes comparable to the particles' ampitudes themselves. If we think of the difference in the amplitudes as the perturbation quantity, we see that there is secular growth of the perturbation, which is proportional to time as long as the perturbation remains small compared to the orbit amplitude. We expect that for a beam slice subject only to an axisymmetric force, but initially displaced from the axis, phase mixing among particles of different oscillation frequency will eventually return the slice to axisymmetry. In an idealized simulation with an infinite number of particles, this process could be well modeled for an indefinite time; the growing individual particle perturbations would average out when macroscopic quantities were calculated. However, in an actual simulation with N particles per slice, the noise level (for quantities like the mean displacement of a slice) is of the order of $\bar{\varepsilon}N^{-1/2}$, where $\bar{\varepsilon}$ is a typical perturbation amplitude for an individual particle. Since $\bar{\varepsilon} \propto t$, the noise eventually comes to dominate at a time t which scales as $N^{1/2}$. Thus increasing N delays the breakdown of the linearized model, but eventually the phase mixing process is overwhelmed by a growing noise signal. We illustrate this behavior by running a simulation of a single slice in which the magnetic pinch force is calculated from Amperes law for a fixed Bennett distribution of current, i.e., $J_0(r) = J_0(1 + r^2/a^2)^{-2}$, giving a force $F(r) = -e^2 J_0 r(1 + r^2/a^2)^{-1}$. The beam profile initially is taken to be a similar Bennett profile displaced from the axis. Figure 2 shows the time behavior of the beam centroid y, for two cases which differ only in the number N of simulation particles. As N increases, the time that the simulation matches the correct physics (steadily decaying oscillations of y) increases as expected. At late times, the noise appears to grow as $tN^{-1/2}$ and, in all cases, dominates the simulation at late enough times.

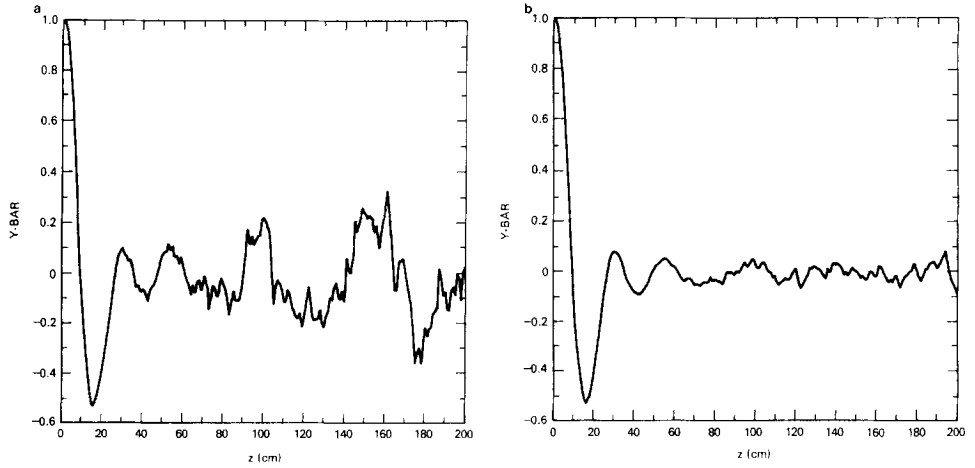

FIG. 2. Mean displacement of a beam slice in a fixed Bennett potential as a function of propagation distance. The coarse graining algorithm was *not* employed. (a) A slice containing 1000 rings, (b) a slice containing 10,000 rings.

Not all particle orbits exhibit secular behavior at the same rate. A Bennett-like potential is nearly harmonic close to the beam axis. Particles whose orbits lie in this region show very slow secular behavior while particles which make large excursions in radius, i.e., those with high perpendicular energy but small angular momentum, show the fastest secular growth in a stationary potential.

For the hose instability, which is convective, the macroscopic beam perturbations at any given location ζ in the beam grow, saturate and then decay. The growth phase is well modeled in a linearized simulation of the type we are discussing, since the exponential growth of the ordered motion easily overwhelms the secular growth of the noise. However, the saturation and decay cannot be modeled by our straightforward linearized simulation unless an extremely large number of particles are employed. If the simulation is to be useful, some method of eliminating the effect of the secularities must be used.

To eliminate the secular growth of the noise, it suffices to break up the ordered secular growth of the individual particle perturbations. In general, we have no interest in individual particle dynamics, but only in the various macroscopic moments. Furthermore, every particle ring carries with it both axisymmetric attributes—x, y, v_x, v_y, γ—that determine the position and motion of the ring and the transport of information from one radial region to another by means of large scale particle orbits, and linearized attributes—$\varepsilon_x^{\mathrm{I}}, \varepsilon_x^{\mathrm{II}}, \varepsilon_y^{\mathrm{I}}, \varepsilon_y^{\mathrm{II}}, \dot{\varepsilon}_x^{\mathrm{I}}, \dot{\varepsilon}_x^{\mathrm{II}}, \dot{\varepsilon}_y^{\mathrm{I}}, \dot{\varepsilon}_y^{\mathrm{II}}$—that carry the perturbation information. The problem of secularities affects only the linearized quantities. Our task is thus to find some technique that preserves the unperturbed orbits and the present value of the macroscopic quantities, but somehow averages out the perturbed quantities pertaining to the individual particles before they have the opportunity to grow intolerably large. In particular, the beam property that acts as the source for the electromagnetic field equations is the axial component $J_z(r, \zeta, z)$ of current density, which is equal to $c\rho(r, \zeta, z)$, where ρ is the charge density, since all particles have $v_z = c$.

We have developed a technique that we call "coarse graining" that accomplishes these objectives. Basically, this consists of periodically performing averages of all the perturbed quantities ε and $\dot{\varepsilon}$ over all the particles in a given cell in configuration space. The ε's and $\dot{\varepsilon}$'s for all of these particles are then reset to the average value at that cell. The averages are weighted in such a way that the perturbed current density $J_z^{\mathrm{II}}(r, \zeta, z)$ is left unchanged. The process is similar to one of the techniques of "local reconstruction" suggested by Friedman, Denavit and Sudan [14]. We believe that this process is faithful to the physics of the hose instability. Since the instability is basically fluid-like, it is driven by the macroscopic quantity $J_z^{\mathrm{II}}(r, \zeta, z)$, which is preserved each time the phase-space is coarse grained. On the other hand, the essential feature of phase-mixing is preserved, since the unperturbed orbits are not altered in any way. The coarse graining technique would probably not be appropriate to resonant micro-instabilities, since resonant wave-particle interactions would be disrupted. The algorithm for performing the coarse graining is presented in detail in Appendix B.

The coarse graining should be performed at intervals which are long compared to

the individual simulation time steps, but short compared to the times for secular growth. Since the oscillation period of typical particles in the axisymmetric potential well (the "betatron period") is the characteristic time for doubling of the initial individual particle ε's, it is suggested that the coarse graining interval be of the order of the betatron period. Of course the macroscopic time evolution must be insensitive to the exact choice of coarse graining interval, if the results are to be meaningful.

To illustrate the technique, the problem of a single displaced beam slice subject to a fixed Bennett potential—Fig. 2—was rerun on the code with coarse graining.

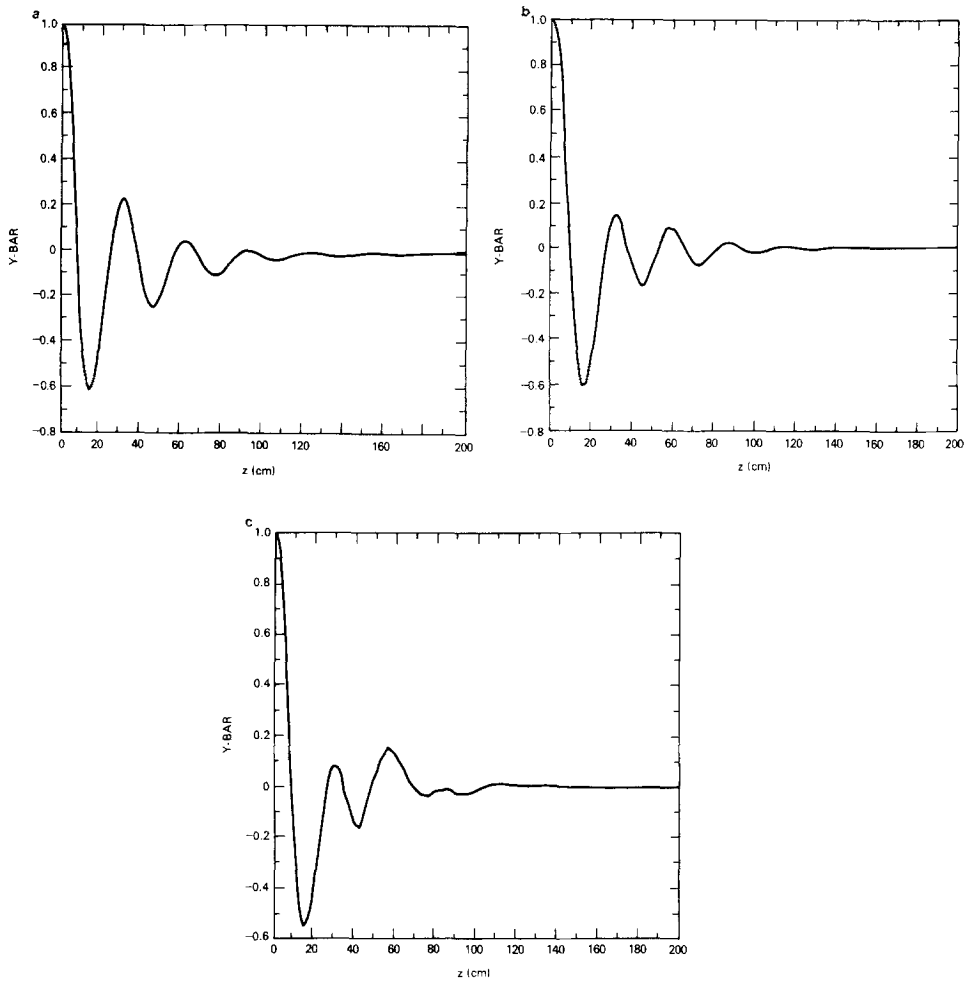

FIG. 3. Mean displacement of a beam slice in a fixed Bennett potential as a function of propagation distance. The coarse graining algorithm was employed. Each slice contained 1000 rings. The coarse graining was applied every (a) 10 time steps, (b) 20 time steps, (c) 30 time steps.

The averaging process was carried out at various intervals. For intervals between about 0.5 to 1.5 betatron periods, the results were insensitive to the averaging frequency, as shown in Fig. 3. The displacement dies out in a manner similar to that without coarse graining, but the late-time noise which was seen in the previous figure does not reappear.

For static potentials, the coarse graining algorithm we have described works quite well. When the potential varies in time, as it does in the problems of interest, where beam perturbations self-consistently drive the fields for instability modes like the resistive hose, another effect can prove troublesome numerically. Chambers [15] and Friedman *et al.* [14] have shown that a few particles experience almost exponential growth of their perturbed quantities ε, in a stochastic way that is nearly impossible to resolve in simulations. Furthermore, this effect can be spread to a large number of particles by the coarse graining algorithm. We deal with this problem in an ad hoc way which seems to have only a minimal effect on the system as a whole. At each time step we determine which ring in the slice has the largest value of ε. We replace the ε and $\dot{\varepsilon}$ of this ring with values averaged over all the particles in the slice. This replacement tends to make the slice behave slightly more like a rigid beam, but at each time step affects only one particle in about 2000.

The effect of applying both algorithms is a linearized particle code which can treat the hose instability in a way which accurately reproduces the growth, saturation and decay. Figure 4 shows the result of a hose simulation with SIMM1, including coarse graining. We note that at any given location ζ in the beam, the mode grows (in good agreement with linear theory [7]) saturates and then decays;

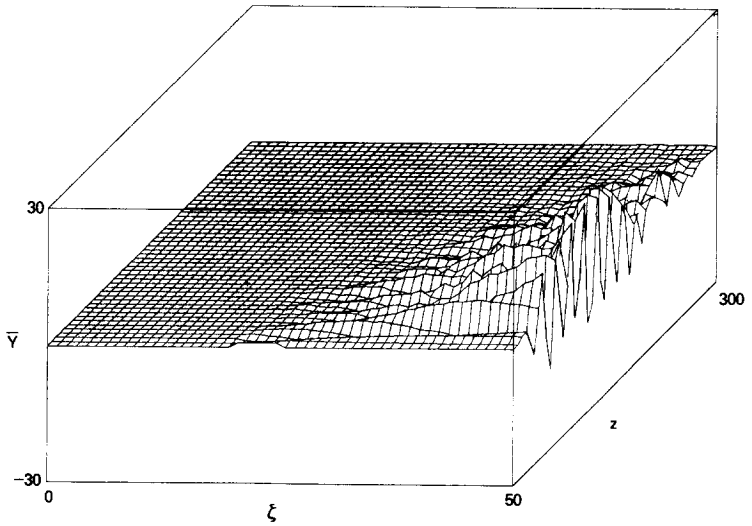

FIG. 4. Surface plot of the hose displacement $\bar{y}$ as a function of the distance back from the beam head ζ and propagation distance, z. The coarse graining algorithm was applied every 20 steps. The convective nature of the instability was preserved in the simulation.

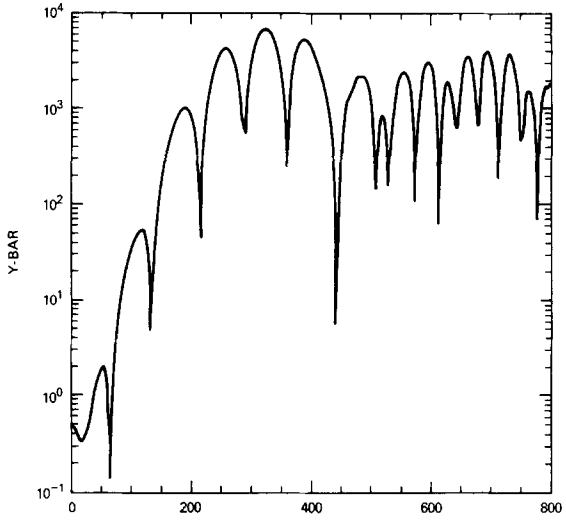

FIG. 5. Hose displacement $\bar{y}$ as a function of propagation distance z for a slice of the beam of the simulation of an unstable beam far behind the beam head. The hose amplitude grows, saturates, and eventually decays. The shift to higher frequencies at late times is a real effect due to variation of the beam radius from head to tail; it will be discussed elsewhere.

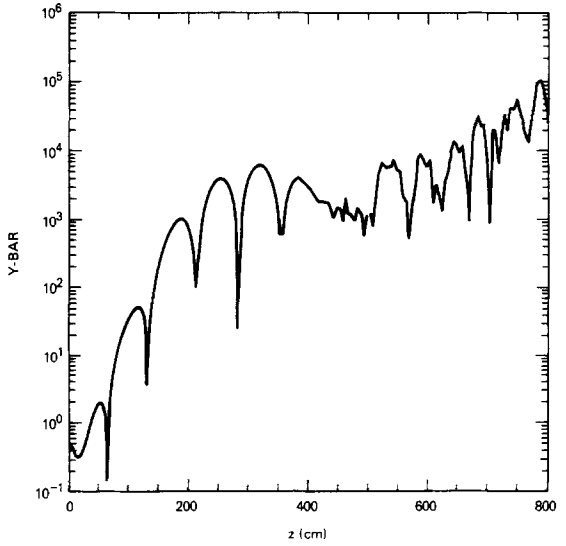

FIG. 6. Hose displacement $\bar{y}$ as a function of propagation distance z for a beam slice of a simulation identical to that of Fig. 5, but without coarse graining algorithm. The hose amplitude grows, saturates, and then regrows due to secular growth effects.

as a function of z, the mode continues to grow convectively backward in ζ. Figure 5 shows the displacement of a single slice far behind the beam head. The meaningful results shown in Figs. 4 and 5, i.e., growth rates, saturation point, peak amplitude, extent of decay, are quite insensitive to variations in the coarse graining interval, as long as it is within, say, 0.5 to 1.5 mean betatron periods. However, minor variations in, e.g., individual oscillation peaks can be detected. Fig. 6 shows the results of an identical run without coarse graining or averaging out the largest ε. For this case, the mode grows as before but after it saturates, the seculiar behavior becomes dominant and the displacements continue to grow without bound.

Appendix A

The field equations used in SIMM1 are the reduced set of Maxwell's equations derived by Lee [13]. Using the paraxial approximation and ζ instead of z as an independent variable, we can write

$$\nabla_\perp^2 \mathbf{A}_\perp = -(4\pi/c)\mathbf{J}_\perp,$$

$$\nabla_\perp^2 A_z = -\frac{4\pi}{c} J_z,$$

$$\nabla_\perp^2 \phi = -4\pi\rho,$$

$$\nabla_\perp \cdot \mathbf{J}_\perp - \frac{\partial J_z}{\partial \zeta} + \frac{\partial c\rho}{\partial \zeta} = 0,$$

$$\nabla_\perp \cdot \mathbf{A}_\perp - \frac{\partial A_z}{\partial \zeta} + \frac{\partial \phi}{\partial \zeta} = 0,$$

where $\mathbf{A}$ is the vector potential, ϕ is the scalar potential, the subscript z is associated with the axial direction and the subscript $\perp$ is associated with the radial variables r and θ.

The electromagnetic fields can be obtained from

$$\mathbf{E}_\perp = -\frac{\partial \mathbf{A}_\perp}{\partial \zeta} - \nabla_\perp \phi,$$

$$E_z = -\frac{\partial A_z}{\partial \zeta} + \frac{\partial \phi}{\partial \zeta},$$

$$\mathbf{B}_\perp = -\hat{e}_z \times \left(\nabla_\perp A_z + \frac{\partial \mathbf{A}_\perp}{\partial \zeta} \right),$$

$$B_z = (\nabla_\perp \times \mathbf{A})_z,$$

$$\mathbf{J}_\perp = \sigma \mathbf{E}_\perp,$$

$$J_z = J_{bz} + \sigma E_z.$$

The field equations simplify further if we drop the transverse displacement current and write

$$\mathbf{E}_\perp = -\nabla_\perp \phi.$$

Then the field equations can be written as

$$\nabla_\perp^2(\mathscr{A} + \phi) = -\frac{4\pi}{c}\left(J_{bz} - \sigma\frac{\partial \mathscr{A}}{\partial \zeta}\right),$$

and

$$\nabla_\perp^2 \frac{\partial \mathscr{A}}{\partial \zeta} = \nabla \cdot \frac{4\pi\sigma}{c}\nabla_\perp \phi,$$

where

$$\mathscr{A} = A_z - \phi.$$

We introduce cylindrical coordinates, and make a linearized multipole decomposition of the azimuthal dependence. Then

$$J_{bz} = J_b^0 + J_{bo}^1 \sin\theta,$$
$$\sigma = \sigma^0 + \sigma^1 \sin\theta,$$
$$\mathscr{A} = \mathscr{A}^0 + \mathscr{A}^1 \sin\theta,$$
$$\phi = \phi^0 + \phi^1 \sin\theta,$$

if we consider only displacements along the y axis.

The field equations are

$$\frac{1}{r}\frac{\partial}{\partial r} r \frac{\partial}{\partial r}(\mathscr{A}^0 + \phi^0) = -\frac{4\pi}{c}\left(J_b^0 - \sigma^0 \frac{\partial \mathscr{A}^0}{\partial \zeta}\right),$$

$$\frac{1}{r}\frac{\partial}{\partial r} r \frac{\partial \mathscr{A}^0}{\partial r \partial \zeta} = \frac{1}{r}\frac{\partial}{\partial r} r \frac{4\pi\sigma^0}{c}\frac{\partial \phi^0}{\partial r},$$

and

$$\frac{\partial}{\partial r}\frac{1}{r}\frac{\partial}{\partial r} r (\mathscr{A}^1 + \phi^1) = -\frac{4\pi}{c}\left(J_b^1 - \sigma^0 \frac{\partial \mathscr{A}^1}{\partial \zeta} - \sigma^1 \frac{\partial \mathscr{A}^0}{\partial \zeta}\right),$$

$$\frac{\partial}{\partial r}\frac{1}{r}\frac{\partial}{\partial r} r \frac{\partial \mathscr{A}^1}{\partial \zeta} = \frac{1}{r}\frac{\partial}{\partial r} r \left(\frac{4\pi\sigma^0}{c}\frac{\partial \phi^1}{\partial r} + \frac{4\pi\sigma^1}{c}\frac{\partial \phi^0}{\partial r}\right) - \frac{4\pi\sigma^0}{c}\frac{\phi^1}{r^2}.$$

The code determines the conductivity from the linearized version of

$$\frac{\partial \sigma}{\partial \zeta} = K J_b + \gamma_i \frac{\sigma}{c} - \beta_r \sigma^2,$$

where, if the propagation medium is air, we use the rough model [16],

$$\kappa = 8.5 \times 10^{-4} \text{ cm/statcoulomb},$$

$$\beta_r = 7.0 \times 10^{-15} \text{ sec/cm},$$

and

$$\gamma_i = [A\rho S^3/(1 + BS + CS^2 + DS^3)] \text{ sec}^{-1},$$

where

$$S \equiv E^2/\rho^2,$$

E is the electric field in statvolts/cm, ρ is the air density in atmospheres, and

$$A = 1.42 \times 10^{-4}$$

$$B = 9.18 \times 10^{-6},$$

$$C = 2.66 \times 10^{-10},$$

$$D = 2.82 \times 10^{-17}.$$

One could envision improving this model in a variety of ways, such as making κ and β_r temperature-independent, including attachment, including the effects of various minority species and chemical changes in complex gases such as air, and modeling nonlocal or magnetic field dependent conductivity if the electron mean free path is long compared to the macroscopic lengths or Larmor radii.

Appendix B

Consider the equation for $J_z^{II}(r, \zeta)$ rewritten as

$$J_z^{II}(r, \zeta) = \frac{-cq}{2\pi r} \sum_{N_s} \sum_{k \in N_s} S_r(r_k^0; r - r_k^0),$$

$$[(\varepsilon_{kx}^{I} \sin \alpha_k - \varepsilon_{ky}^{I} \cos \alpha_k) \cos \alpha_k \, (\varepsilon_{kx}^{II} \sin \alpha_k - \varepsilon_{ky}^{II} \cos \alpha_k)]$$

$$- \frac{cq}{2\pi r} \frac{\partial}{\partial r} \sum_{k \in N_s} S_r(r_k^0; r - r_k^0),$$

$$[(\varepsilon_{kx}^{I} \cos \alpha_k + \varepsilon_{ky}^{I} \sin \alpha_k) \sin \alpha_k + (\varepsilon_{kx}^{II} \cos \alpha_k + \varepsilon_{ky}^{II} \sin \alpha_k) \cos \alpha_k],$$

where the first summation is over all particles in cell N_s and the second summation is over cells.

The two quantities which must be preserved by the averaging process are

$$F_{k1} = (\varepsilon_{kx}^{I} + \varepsilon_{ky}^{II}) \sin \alpha_k \cos \alpha_k - \varepsilon_{ky}^{I} \cos^2 \alpha_k - \varepsilon_{kx}^{II} \sin^2 \alpha_k,$$

$$F_{k2} = (\varepsilon_{ky}^{I} + \varepsilon_{ky}^{II}) \sin \alpha_k \cos \alpha_k - \varepsilon_{ky}^{I} \sin^2 \alpha_k - \varepsilon_{kx}^{II} \cos^2 \alpha_k.$$

Recall that, in the average, only the ε's are changed. The quantities α_k and $S_r(r_k^0, r - r_k^0)$ depend on axisymmetric variables and are the same before and after the averages. If F_{k1} and F_{k2} are preserved in the average so are linear combinations of them. In particular

$$F_{k2} - F_{k1} = \varepsilon_{ky}^{\mathrm{I}} + \varepsilon_{kx}^{\mathrm{II}},$$

and

$$F_{k1} + F_{k1} = (\varepsilon_{kx}^{\mathrm{II}} + \varepsilon_{ky}^{\mathrm{II}}) \sin 2\alpha_k + (\varepsilon_x^{\mathrm{II}} - \varepsilon_y^{\mathrm{I}}) \cos 2\alpha_k$$

will be unchanged. If we choose to average in such a way that $\varepsilon_{ky}^{\mathrm{I}} + \varepsilon_{kx}^{\mathrm{II}}$, $(\varepsilon_{kx}^{\mathrm{II}} - \varepsilon_{ky}^{\mathrm{I}}) \cos 2\alpha_k$, $\varepsilon_{kx}^{\mathrm{I}} \sin 2\alpha_k$, and $\varepsilon_{ky}^{\mathrm{II}} \sin 2\alpha_k$ are preserved then F_{k1} and F_{k2} will be unchanged.

Let

$$\delta_{k1} = \varepsilon_{kx}^{\mathrm{II}} + \varepsilon_{ky}^{\mathrm{I}}$$

and

$$\delta_{kz} = \varepsilon_{ky}^{\mathrm{I}} - \varepsilon_{kx}^{\mathrm{II}},$$

then the averages can be written as

$$\bar{\delta}_1 = \sum_{k \in N_s} \delta_{k1} \Big/ \sum_{k \in N_s},$$

$$\bar{\delta}_2 = \sum_{k \in N_s} \delta_{kz} \cos 2\alpha_k \Big/ \sum_{k \in N_s} \cos 2\alpha_k,$$

and

$$\bar{\varepsilon}_y^{\mathrm{I}} = 1/2(\bar{\delta}_1 + \bar{\delta}_2),$$

$$\bar{\varepsilon}_y^{\mathrm{I}} = 1/2(\bar{\delta}_1 - \bar{\delta}_2),$$

while

$$\bar{\varepsilon}_x^{\mathrm{I}} = \sum_{k \in N_s} \varepsilon_{kx}^{\mathrm{I}} \sin 2\alpha_k \Big/ \sum_{k \in N_s} \sin 2\alpha_k,$$

$$\overline{\varepsilon_y^{\mathrm{II}}} = \sum_{k \in N_s} \varepsilon_{ky}^{\mathrm{II}} \sin 2\alpha_k \Big/ \sum_{k \in N_s} \sin 2\alpha_k.$$

Finally, we associate the averages with the ε's of individual rings by using the particle shape functions.

In addition to averaging over the ε's, some method must be employed to average the $\bar{\varepsilon}$'s. The method which suggests itself is to form averages which preserve J_z. These averages depend not only on the particle shapes and positions but also on the rotation velocity of the rings. In practice, these averages, especially at small radii, tend to be dominated by a few rapidly spinning rings. As a compromise,

we have chosen to perform unweighted averages of $\dot{\varepsilon}_x^{\mathrm{I}}$, $\dot{\varepsilon}_y^{\mathrm{I}}$, $\dot{\varepsilon}_x^{\mathrm{II}}$, and $\dot{\varepsilon}_y^{\mathrm{II}}$. We have performed a number of tests on the $\dot{\varepsilon}$ averages and the method appears to be satisfactory.

ACKNOWLEDGMENTS

The authors would like to acknowledge useful conversations with Drs. Richard Hubbard and Steve Slinker and with Dr. Frank Chambers. This work was supported by the Defense Advanced Research Projects Agency under ARPA Order 4395, Amendment Number 41, and monitored by Naval Surface Weapons Center.

REFERENCES

1. R. J. BRIGGS, J. C. CLARK, T. J. FESSENDEN, R. E. HESTER, AND E. J. LAUER, *in* "Proc. of the Second Intl. Conf. on High Power Electron and Ion Beam Research and Technology," p. 319, Cornell University, Ithaca, New York, 1977.
2. M. N. ROSENBLUTH, *Phys. Fluids* **3** (1960), 932.
3. S. WEINBERG, *J. Math. Phys.* **5** (1964), 1371.
4. E. P. LEE, *Phys. Fluids* **21** (1978), 1327.
5. H. S. UHM AND M. LAMPE, *Phys. Fluids* **23** (1980), 1574.
6. W. M. SHARP, M. LAMPE, AND H. S. UHM, *Phys. Fluids* **25** (1982), 1456.
7. M. LAMPE, W. M. SHARP, R. F. HUBBARD, E. P. LEE, AND R. H. BRIGGS, *Phys. Fluids* **27** (1984), 2921; M. LAMPE, W. M. SHARP, AND R. F. HUBBARD, NRL Memo Report 5140, 1984.
8. E. P. LEE, F. W. CHAMBERS, L. L. LODESTRO, AND S. S. YU, *in* "Proc. of the Second Intl. Conf. on High Power Electron and Ion Beam Research and Technology," p. 381, Cornell University, Ithaca, New York, 1977.
9. M. LAMPE, G. JOYCE, AND R. F. HUBBARD, *in* "Proc. of the Fifth Intl. Conf. on High Power Electron and Ion Beam Research and Technology, p. 336, San Francisco, Calif., 1983.
10. A. FRIEDMAN, R. N. SUDAN, AND J. DENAVIT, *J. Comp. Phys.* **40** (1981), 1.
11. F. CHAMBERS, J. MASAMITSU, AND E. P. LEE, Lawrence Livermore National Laboratory, Report UCID-1949L, 1982.
12. G. JOYCE AND M. LAMPE, *Phys. Fluids* **26** (1983), 3377.
13. E. P. LEE, Lawrence Livermore National Laboratory, Report UCID-17286, 1976.
14. A. FRIEDMAN, J. DENAVIT, AND R. N. SUDAN, *J. Comput. Phys.* **44** (1981), 104.
15. F. CHAMBERS, Private communication, 1983.
16. F. W. CHAMBERS, Lawrence Livermore National Laboratory, Report UCID-18302, 1979.